CDDpress

www.nature.com/cddiscovery

ARTICLE OPEN

Rapid degeneration of iPSC-derived motor neurons lacking *Gdap1* engages a mitochondrial-sustained innate immune response

Marian León[1], Javier Prieto[1,2], María Micaela Molina-Navarro[1], Francisco García-García[3], Manuela Barneo-Muñoz[4], Xavier Ponsoda[1], Rosana Sáez[1], Francesc Palau[5,6], Joaquín Dopazo[6,7,8], Juan Carlos Izpisua Belmonte[2,10] and Josema Torres[1,9]✉

Charcot-Marie-Tooth disease is a chronic hereditary motor and sensory polyneuropathy targeting Schwann cells and/or motor neurons. Its multifactorial and polygenic origin portrays a complex clinical phenotype of the disease with a wide range of genetic inheritance patterns. The disease-associated gene *GDAP1* encodes for a mitochondrial outer membrane protein. Mouse and insect models with mutations in Gdap1 have reproduced several traits of the human disease. However, the precise function in the cell types affected by the disease remains unknown. Here, we use induced-pluripotent stem cells derived from a *Gdap1* knockout mouse model to better understand the molecular and cellular phenotypes of the disease caused by the loss-of-function of this gene. Gdap1-null motor neurons display a fragile cell phenotype prone to early degeneration showing (1) altered mitochondrial morphology, with an increase in the fragmentation of these organelles, (2) activation of autophagy and mitophagy, (3) abnormal metabolism, characterized by a downregulation of Hexokinase 2 and ATP5b proteins, (4) increased reactive oxygen species and elevated mitochondrial membrane potential, and (5) increased innate immune response and p38 MAP kinase activation. Our data reveals the existence of an underlying Redox-inflammatory axis fueled by altered mitochondrial metabolism in the absence of *Gdap1*. As this biochemical axis encompasses a wide variety of druggable targets, our results may have implications for developing therapies using combinatorial pharmacological approaches and improving therefore human welfare.

Cell Death Discovery (2023)9:217 ; https://doi.org/10.1038/s41420-023-01531-w

INTRODUCTION

Charcot-Marie-Tooth (CMT) disease is the most prevalent hereditary sensory and motor neuropathy (1 in 2500). CMT disease is a clinically and genetically heterogeneous group of disorders sharing common phenotypical features, including weakness, and wasting of distal limb muscles, waned deep tendon reflexes, distal sensory loss, and skeletal deformities. Overall, the clinical traits of the disease result from progressive loss of sensory and motor nerves; affecting either the myelin shaft (CMT type 1 and 4, demyelinating) or the axon (CMT types 2-4, axonal) of motor neurons (MNs). Together, these cellular and structural defects lead to a progressive decrease in patient welfare [1–5].

Several pathological mechanisms underlying CMT2 subtypes have been described, and include defects in mitochondrial dynamics, organelle-organelle contacts, and axonal transport [6]. This pathological diversity has likely been the cause precluding CMT2 from common drug-based therapeutics [1], supporting the notion of personalized medicine as the most viable treatment strategy.

The CMT-associated gene *Ganglioside-induced Differentiation-Associated Protein 1* (*GDAP1*, MIM 606598), encodes an integral mitochondrial outer membrane protein expressed predominantly in MNs and Schwann cells [7, 8]. Similar to our *Gdap1* knockout cellular model, which renders no functional protein, previous research has defined that disease-associated missense mutations in *GDAP1* result in a premature stop codon and a shortened protein [9–14]. GDAP1 protein participates in cellular processes linked to mitochondrial function, including mitochondrial dynamics [8, 10, 15], regulation of glutathione concentration [16, 17], oxidative stress [18], mitochondrial membrane potential [17] and mitochondrial calcium buffering and defects in the mitochondria-lysosomes membrane contacts [19–21]. Although mouse [22, 23] and fly [24] models with mutations in *Gdap1* have reproduced several traits found in human CMT disease, the precise function of GDAP1 in healthy settings and its mechanistic link to CMT disease remains uncertain [25–28]. To address this, we differentiated iPSCs generated from *Gdap1*$^{-/-}$ mice into MNs and found that absence of this protein results in a fragile phenotype

[1]Departamento Biología Celular, Biología Funcional y Antropología Física, Universitat de València, Burjassot, 46100 València, Spain. [2]Gene Expression Laboratory, Salk Institute for Biological Studies, La Jolla, CA 92037, USA. [3]Unidad de Bioinformática y Bioestadística, Centro de Investigación Príncipe Felipe, 46012 València, Spain. [4]Unitat Predepartamental de Medicina, Universidad Jaume I, Castellón de la Plana, Castellón, Spain. [5]Institut de Recerca and Hospital San Joan de Déu, 08950 Barcelona, Spain. [6]CIBER de Enfermedades Raras (CIBERER), ISCIII, Madrid, Spain. [7]Computational Medicine Platform, Andalusian Public Foundation Progress and Health-FPS, 41013 Sevilla, Spain. [8]Institute of Biomedicine of Seville, IBiS, University Hospital Virgen del Rocío/CSIC/University of Seville, Seville, Spain. [9]Instituto de Investigación Sanitaria (INCLIVA), 46010 València, Spain. [10]Present address: Altos Labs, 5510 Morehouse Drive, San Diego, CA 92121, USA. ✉email: josema.torres@uv.es

Received: 20 October 2022 Accepted: 22 June 2023
Published online: 01 July 2023

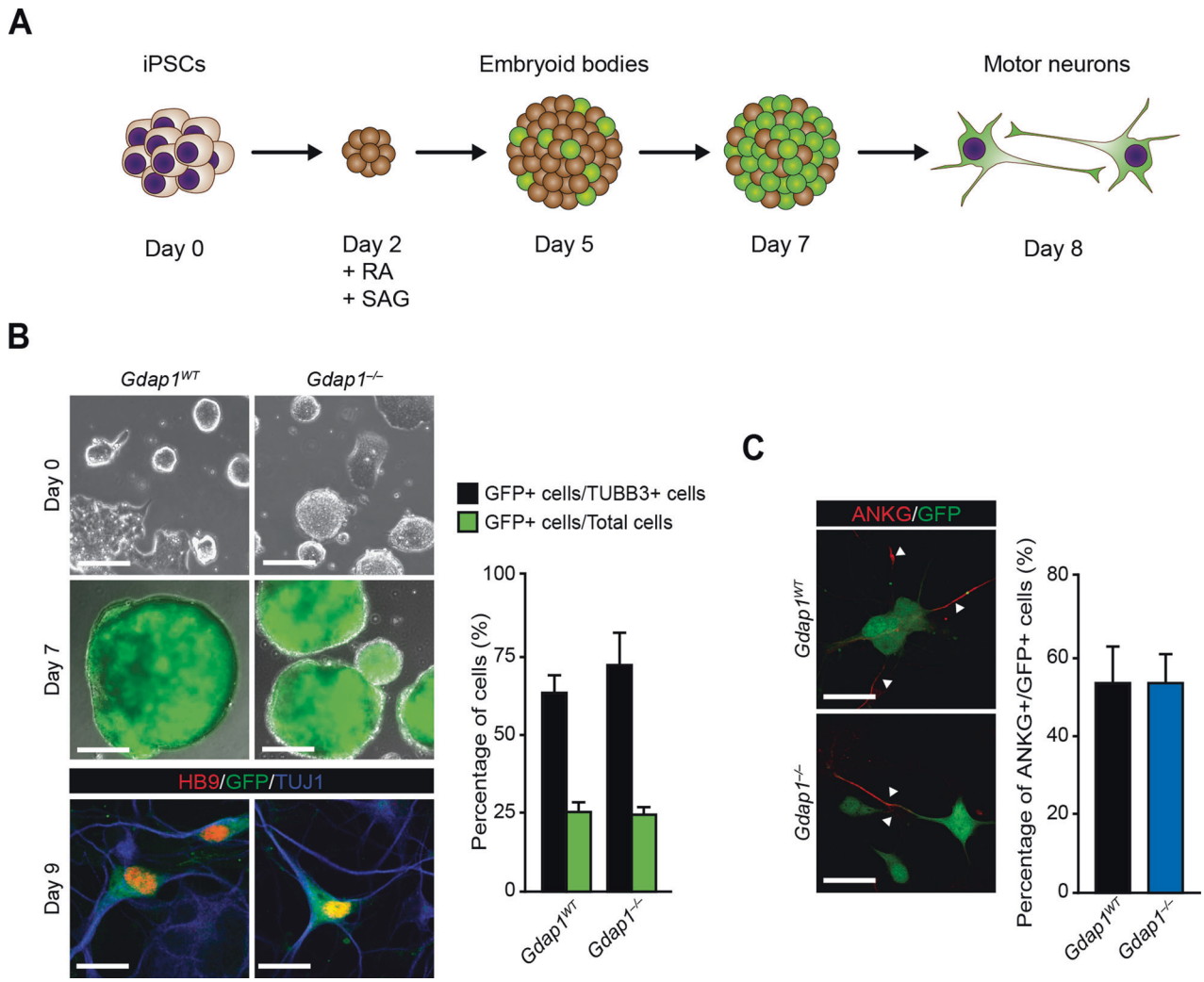

Fig. 1 MN differentiation efficiency of *Gdap1*^{WT} and *Gdap1*$^{-/-}$ iPSCs was similar. A Schematics of iPSCs MN differentiation. Retinoic acid (RA) and smoothened agonist (SAG) are indicated. **B** Upper panels, phase contrast images of undifferentiated iPSC. Middle panels, fluorescence (EGFP, green) and phase contrast merged images of EBs at d7 of differentiation. Lower panels, confocal images of MNs 2 days after plating (d9) stained with indicated antibodies. Bars, 130 µm, 500 µm, and 20 µm, respectively. Right graph, percentage of EGFP-positive cells relative to either Tbb3-positive cells (black bars) or total cells (green bars) ($n = 3$). **C** Left: confocal images of d9 MNs stained with indicated antibodies. Bars, 20 µm. Right graph, percentage of ANKG-EGFP double positive cells relative to total EGFP-positive cells. Data are represented as mean ± SEM from at least three experiments. No statistical significance between genotypes was observed (one-tailed Student's *t*-test).

characterized by mitochondrial dysfunction and activation of the innate immune response.

RESULTS

Gdap1^{WT} and *Gdap1*$^{-/-}$ iPSCs show similar potential for differentiation to mature MNs

To facilitate the identification of MNs in our studies we generated reporter iPSC lines by introducing EGFP under the control of the *Mnx1* (also known as *Hb9*) promoter [29] in *Gdap1*^{WT} and *Gdap1*$^{-/-}$ iPSCs [30]. MN differentiation was induced by retinoic acid (RA) and Smoothened agonist (SAG) stimulation for 1 week (Fig. 1A) [29, 31]. On day (d) 5, we detected EGFP expression and, on d7, embryoid bodies (EBs) were enzymatically disaggregated and cells plated in monolayer (Fig. 1B).

Differentiation efficiency was quantified by quantitative RT-PCR (qPCR), flow cytometry and immunofluorescence. On d7, EGFP fluorescent signal (Fig. 1B, middle panels) and *Mnx1* gene expression (Fig. S1A) increased similarly in both genotypes. Importantly, EGFP-positive cells displayed HB9 nuclear staining by immunofluorescence, validating the pMnx1-EGFP reporter (Fig. 1B, lower panels).

We assessed differentiation efficiency by flow cytometry at d7 and found 16% and 19% of EGFP-positive cells in *Gdap1*^{WT} and *Gdap1*$^{-/-}$ cultures, respectively (Fig. S1B). At d9, cultures were analyzed by confocal microscopy, and the percentage of EGFP-positive cells was approximately 25% in both genotypes (Fig. 1B, green bars). At this timepoint, over 60% of EGFP-positive cells co-expressed the neuronal β-tubulin III (TUBB33) (Fig. 1B, black bars) and the neuronal polarization Ankyrin G (ANKG) markers (Fig. 1C) in both genotypes. Importantly, we detected GDAP1 protein expression in *Gdap1*^{WT} cultures at day 7 of differentiation while it was absent in *Gdap1*$^{-/-}$ cells (Fig. S1C). Thus, as ES differentiation into MNs was not 100%, the contribution of other cell lineages to our results cannot be completely ruled out.

Gdap1$^{-/-}$ MNs have an abnormal cellular phenotype

To assess MN viability, 7-day-old EBs were disaggregated and plated at identical densities (Fig. 2A). From the next day onwards, EGFP-positive cells were manually counted for 2 weeks and compared to d8 (100%). While the percentage of EGFP-positive cells decreased over time in both genotypes, the rate of reduction in Gdap1$^{-/-}$ cultures was increased, with no EGFP-positive cells

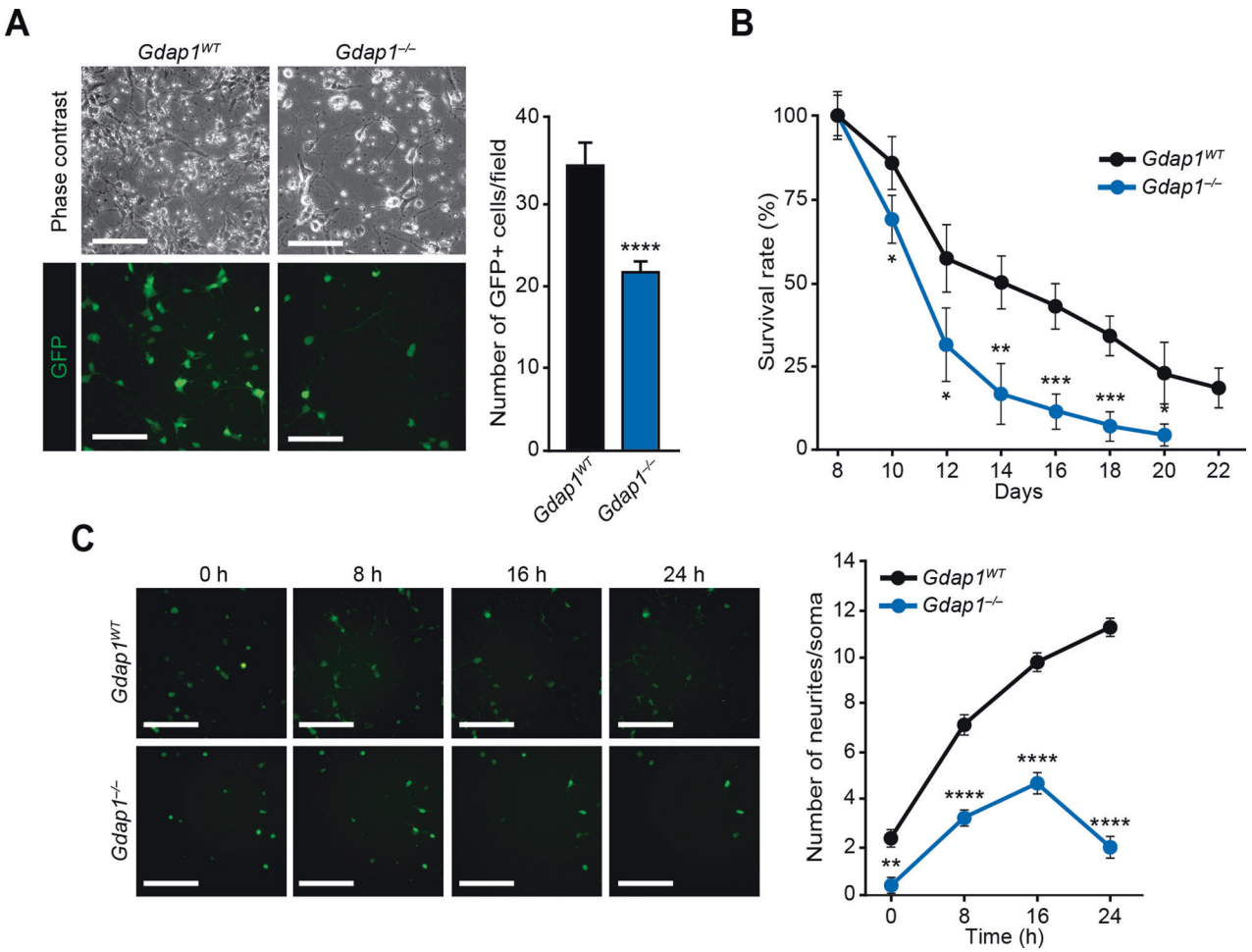

Fig. 2 Abnormal cellular phenotype in *Gdap1*$^{-/-}$ MNs. A Left: phase contrast (top) or fluorescence (bottom) images of differentiated cells one day after plating (d8) at the same density (1.25×10^5 cells/cm^2). Bars, 120 µm. Right: Bar diagram showing average of EGFP-positive cells per field (10 fields per well; $n = 6$ wells per group). **B** Graph showing the survival curve of EGFP-positive cells seeded as in **A**. **C** Left: INCell fluorescence images (EGFP, green) at the indicated times after seeding (d7 of differentiation). Bars, 180 µm. Right: number of neurites per soma in EGFP-positive cells at the indicated times after seeding. Data are represented as mean ± SEM from at least three experiments. Statistical significance between genotypes was assessed with the one-tailed Student's t-test (*$P < 0.05$; **$P < 0.01$; ***$P < 0.001$; ****$P < 0.0001$).

beyond d20 (Fig. 2A, B). To evaluate possible paracrine signaling defects on survival, twice as many *Gdap1*$^{-/-}$ cells were seeded relative to controls (Fig. S2A, B), however this did not change the viability curve. Neurite development of MNs increased rapidly following plating in wild-type controls (Fig. 2C). In contrast, while neurite development initially increased in *Gdap1*$^{-/-}$ MNs, the emergence of neuronal projections stopped at 16 h post-plating and sharply decreased at 24 h (Fig. 2C).

Gdap1$^{-/-}$ MNs show an altered mitochondrial functionality

As GDAP1 is a protein involved in mitochondrial dynamics [8, 32], we investigated whether this process was altered in *Gdap1*$^{-/-}$ iPSC-derived MNs. Mitochondrial morphology (fragmented, tubular, or mixed) in EGFP-positive MN somas was assessed by microscopy using TOM20 as a marker for these organelles (Fig. 3A). MNs of both genotypes displayed mostly fragmented mitochondria. However, *Gdap1*$^{-/-}$ cultures displayed a reduction in cells with tubular mitochondrial morphology, and an increase in those with mixed or fragmented mitochondria (Fig. 3A, middle panels and left graph). The changes in mitochondrial morphology were associated with increased autophagy and mitophagy, assessed by autophagosome LC3B staining, and Pearson Correlation Coefficient (PCC) of TOM20 and LC3B colocalization, respectively (Fig. 3A, right panels, and middle and right graphs). Along these lines, LC3B-II / LC3B-I ratios, assessed by western blot, were increased in differentiated GDAP1-null cells relative to wild-type controls (Fig. S3A). However, no significant differences were observed between genotypes in either mitochondrial mass, measured by immunoblotting for TOM20 (Fig. S3A), or in levels of the machinery governing mitochondrial dynamics in these organelles (Fig. S3B), in agreement with our previous observations in somatic and pluripotent stem cells [30, 33].

We next measured mitochondrial membrane potential (MMP) and mitochondrial superoxide anion, using TMRM and MitoSOX fluorescent probes, respectively. *Gdap1*$^{-/-}$ MNs showed a significant increase of both signals at d7, measured by flow cytometry, and at d8, determined by confocal microscopy (Fig. 3B–E).

Gdap1$^{-/-}$ cells differentiated into MNs display an altered metabolic profile

Oxygen consumption (OCR) and extracellular acidification (ECAR) rates were measured as proxies of oxidative phosphorylation (OXPHOS) and glycolysis, respectively. Data analysis showed higher OCR in *Gdap1*$^{-/-}$ cells compared to controls (Fig. 4A), while glycolysis and glycolytic capacity were considerably lower in *Gdap1*$^{-/-}$ cultures (Fig. 4B).

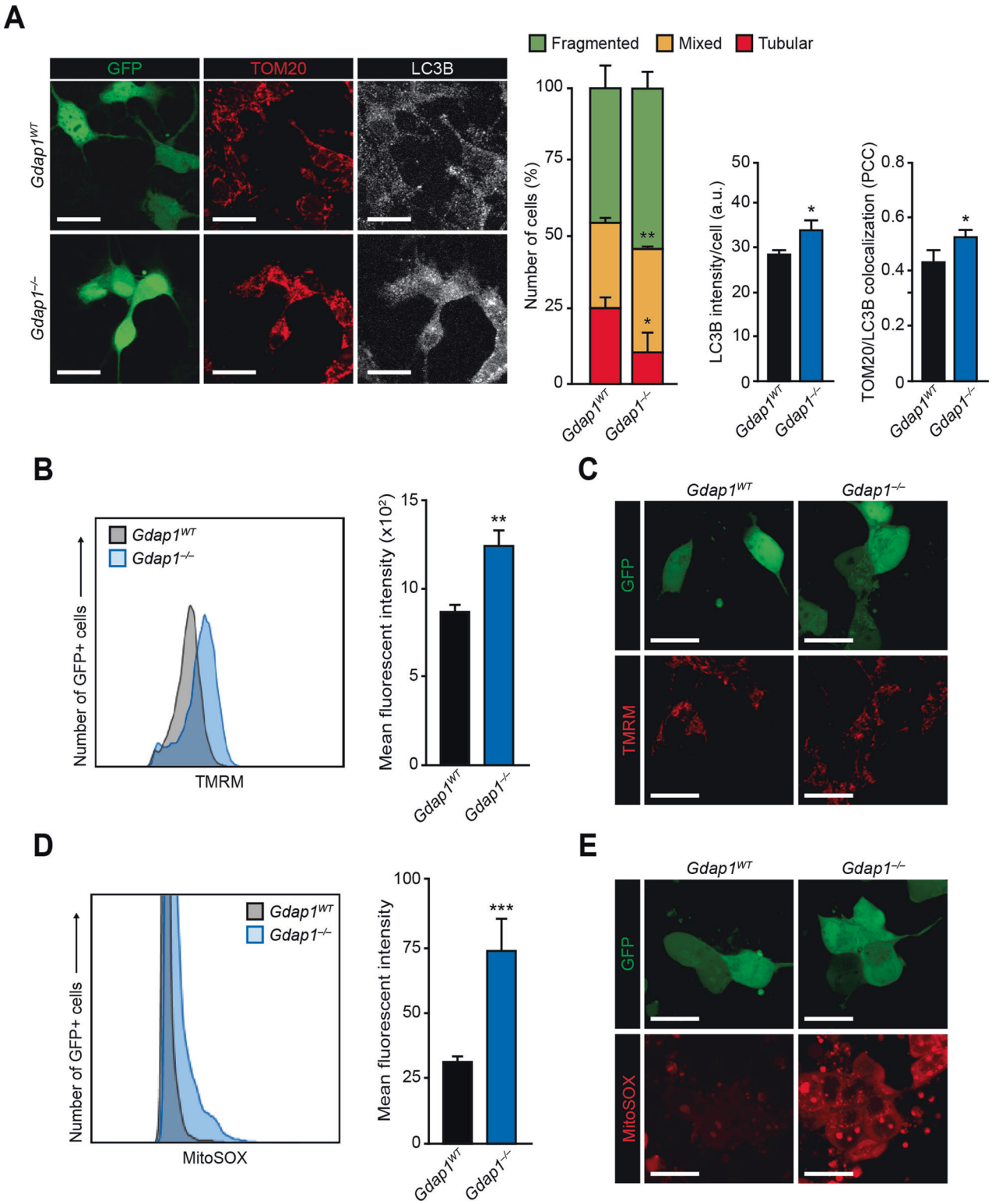

Fig. 3 Altered mitochondrial functionality in *Gdap1*$^{-/-}$ MNs. A Left: confocal images of MNs 2 days after plating (d9) that were fixed and stained with the indicated antibodies. Bars, 20 μm. Right: quantification of the observed mitochondrial morphologies (left graph), LC3B mean signal intensity per cell (middle graph) and colocalization of LC3B and TOM20 assessed by Pearson's correlation coefficient (PCC) of both signals in MNs (right graph). **B** Histogram: TMRM-uptake assessed by flow cytometry of MNs at d7 of differentiation. Graph: quantification of the mean fluorescent intensities of the histograms. **C** Confocal images of MNs 2 days after seeding (d9) that were stained with TMRM. Bars, 15 μm. **D** Histogram: mitochondrial superoxide assessment by flow cytometry analysis in MNs at d7. Graph: quantification of the mean fluorescent intensities in histograms. **E** Confocal images of cultured MNs 2 days after seeding (d9) stained with MitoSOX to detect mitochondrial superoxide. Bars, 15 μm. Data are represented as mean ± SEM from at least three independent experiments. The one-tailed Student's t-test was used to assess statistical significance between genotypes (*$P < 0.05$; **$P < 0.01$; ***$P < 0.001$).

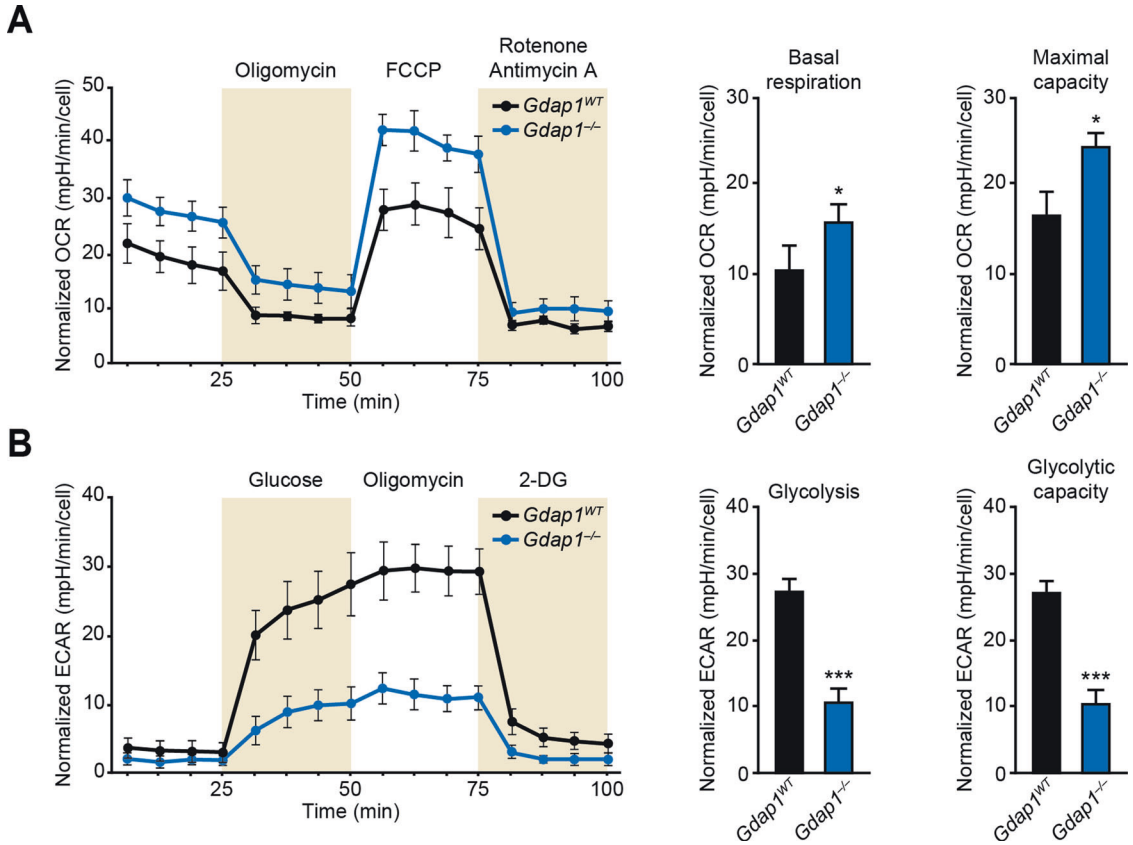

Fig. 4 Increased OXPHOS and decreased glycolysis in *Gdap1*$^{-/-}$ cells differentiated into MNs. A Left: oxygen consumption rates (OCR) in differentiated cultures 1 day after plating (d8 of differentiation) ($n = 6$). Right: graphs showing indicated OCR parameter values. **B** Left: extracellular acidification rates (ECAR) in differentiated cultures 1 day after plating (d8 of differentiation). Right: graphs show the values for the indicated ECAR parameters. Data are represented as mean ± SEM from at least six independent experiments. The one-tailed Student's t-test was used to assess statistical significance between genotypes (*$P < 0.05$; ***$P < 0.001$).

To further investigate these metabolic differences, the major metabolic enzymes involved in OXPHOS or glycolysis were analyzed by immunoblotting. Atp5b subunit (complex V), Hk2 and Ldh enzyme expression decreased in *Gdap1*$^{-/-}$ cultures (Fig. 5A, B). Interestingly, changes in hexokinase genes may participate in development of some CMT subtypes [34–36]. To rule out the possibility that HK2 downregulation was an initial genetic defect in *Gdap1*$^{-/-}$ iPSCs, expression of HK1, HK2 and GDAP1 proteins was measured in undifferentiated iPSCs or during their differentiation into MNs by immunoblotting (Fig. 5C). While kinetics of HK1 expression was similar in both genotypes, expression of HK2 readily declined at d7 of differentiation in *Gdap1*$^{-/-}$ cells (Fig. 5C), when GDAP1 expression is first detected (Fig. S1C).

Gdap1$^{-/-}$ cells differentiated into MNs show an increase of innate immune response markers and activated p38 MAPK

Gene ontology analysis of our previously published transcriptome data [30] revealed that *Gdap1*$^{-/-}$ MEFs displayed marked upregulation of genes associated with innate immune response (Fig. 6A). In agreement with the observed oxidative stress increase in *Gdap1*$^{-/-}$ MNs (Fig. 3B–E), the analysis also showed a drastic activation of markers associated with the cellular response against ROS (Fig. 6A).

Next, gene expression of these markers was analyzed during MN differentiation (Fig. 6B). Gdap1-null cells displayed an upregulation of factors induced by the activation of the innate immune response both at the EB stage (d6 of differentiation; *Il6*, and *Cxcl10*) and after seeding, at d8 (*Dhx58*, *Ddx58*, *Isg15*, *Ifit1* and *Irf7*) and d10 (*Dxd58*, *Ifih1*, *Ddx58*, *Il6*, *Cxcl10*, *Ifi44*, *Isg15*, *Ifit1* and *Irf7*).

A relationship between ROS, innate immune response and MAPK activation does exist [37–39]. Activation of JNK1/2 and ERK1/2 MAPKs was observed in both genotypes during early differentiation (Fig. 7). In wild-type controls, p38α MAPK underwent a mild activation (around 1.5-fold) during differentiation. However, phosphorylation of this MAPK increased by more than 3-fold in Gdap1-null cultures at d3. At d7, the increased activation of p38α remained evident in GDAP1-null relative to control cultures (Fig. 7, right-most graph).

DISCUSSION

In this study, we found that lack of *Gdap1* induces a fragile phenotype in MNs characterized by mitochondrial dysfunction and activation of the innate immune response. Our results provide insight into Gdap1 function in health and disease.

GDAP1 is a protein of the outer mitochondrial membrane described as an accessory protein promoting fission of these organelles [8, 28, 32, 40, 41]. Conversely, our studies show that GDAP1 favors mitochondrial fusion as its absence increased the percentage of MNs with fragmented mitochondria. Further, silencing of *GDAP1* mRNA in SH-SY5Y neuroblastoma cells can induce mitochondrial fragmentation [19] and *Gdap1* deficiency in murine models has mild [21, 23] or almost no effect [22] on mitochondrial size.

Mitochondria are main sources of cellular ROS production [42], and uncontrolled production of ROS can cause fatal damage to cells [43]. By joining functional and dysfunctional mitochondria, cells distribute the contents of these organelles, maintaining homeostasis [44]. Cellular stress can lead to

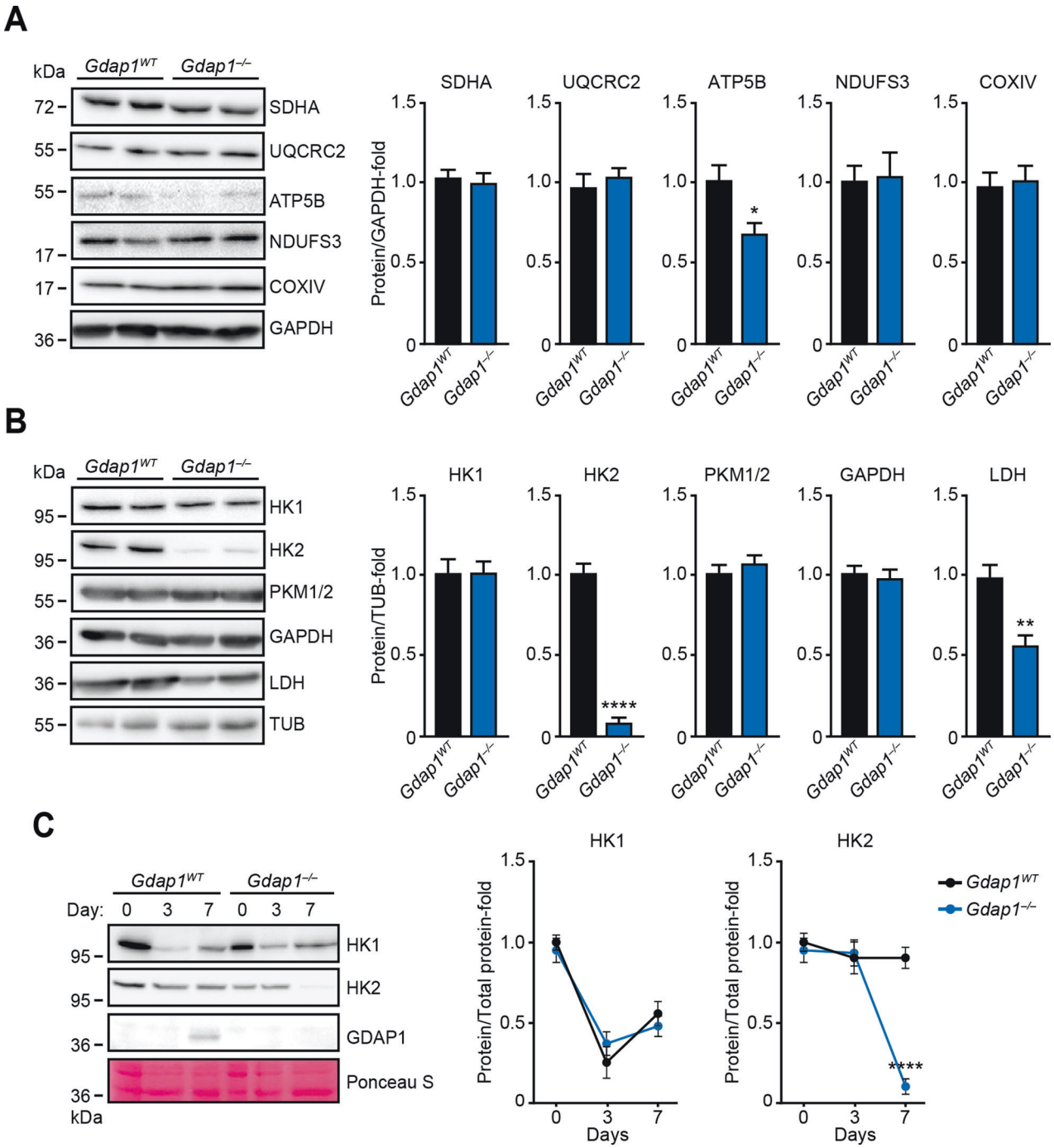

Fig. 5 *Gdap1*$^{-/-}$ cells differentiated into MNs showed altered metabolic enzyme expression. A, **B** Left: cell lysates of EBs at d7 of differentiation were analyzed by immunoblotting using indicated antibodies. Right: graphs showing quantification of immunoblots. **C** Left: cell lysates from undifferentiated iPSCs (day 0), or EBs at the indicated days of differentiation were analyzed by immunoblotting using the antibodies shown. Loading control: Ponceau-S staining. Right: quantification of immunoblots ($n = 3$). Data are represented as mean ± SEM from at least three independent experiments. The one-tailed Student's t-test was used to assess statistical significance between genotypes (*$P < 0.05$; **$P < 0.01$; ****$P < 0.0001$).

overwhelming mitochondrial dysfunction eventually triggering its degradation by mitophagy [45, 46], and mitochondrial fission is necessary for this process [46–49]. Our data show a correlation between increased ROS levels, mitochondrial fragmentation, and mitophagy activation in GDAP1-null MNs, suggesting a loss of mitochondrial functionality due to a rise in oxidative stress.

Defective OXPHOS can generate ROS [50]. *Gdap1*$^{-/-}$ cell cultures showed a decrease in glycolysis associated with HK2 and LDH downregulation, and a rise in oxidative metabolism. While overexpression of GDAP1 induced increased MMP [17], *LDH* silencing can activate OXPHOS in several tumor cell lines [51]. Our results showing the presence of hyperpolarized mitochondria in *Gdap1*$^{-/-}$ MNs suggests that mitochondria may be unable to consume MMP,

A

GO	Pathway	Log of ratio	p-Adjusted	n-genes
GO:0045087	Innate immune response	0.3980	8.20×10^{-07}	289
GO:0034599	Cellular response to oxidative stress	0.6392	7.41×10^{-05}	97
GO:0009615	Response to virus	0.4503	1.69×10^{-04}	168
GO:0034341	Response to interferon-gamma	0.7879	2.22×10^{-04}	57
GO:0048525	Negative regulation of viral processes	1.0545	3.40×10^{-04}	33
GO:0051607	Defense response to virus	0.6179	7.22×10^{-04}	86
GO:0035456	Response to interferon-beta	1.7567	9.94×10^{-04}	23
GO:0035458	Cellular response to interferon-beta	1.7177	1.19×10^{-03}	22
GO:0019883	Antigen processing and presentation of endogenous antigen	1.2905	1.21×10^{-03}	12
GO:0002753	Cytoplasmic pattern recognition receptor signaling pathway	1.4988	4.73×10^{-03}	10
GO:0002483	Antigen processing and presentation of endogenous antigen	1.1870	9.20×10^{-03}	11
GO:0034614	Cellular response to reactive oxygen species	0.6389	9.53×10^{-03}	57
GO:0070301	Cellular response to hydrogen peroxide	0.8030	0.0112	37
GO:0045088	Regulation of innate immune response	0.3945	0.0113	127
GO:0071346	Cellular response to interferon-gamma	0.9788	0.0163	29
GO:0032606	Type I interferon production	0.8740	0.0247	34
GO:0042770	Signal transduction in response to DNA damage	0.4570	0.034	75
GO:0032481	Positive regulation of type I interferon production	0.9515	0.035	22
GO:0007249	I-kappaB kinase/NF-kappaB cascade	0.2725	0.048	203
GO:0000280	Nuclear division	-0.3719	2.68×10^{-07}	334
GO:0007067	Mitosis	-0.3719	2.68×10^{-07}	334
GO:0048285	Organelle fission	-0.3597	2.68×10^{-07}	355
GO:0051301	Organelle division	-0.3104	3.70×10^{-07}	466

B

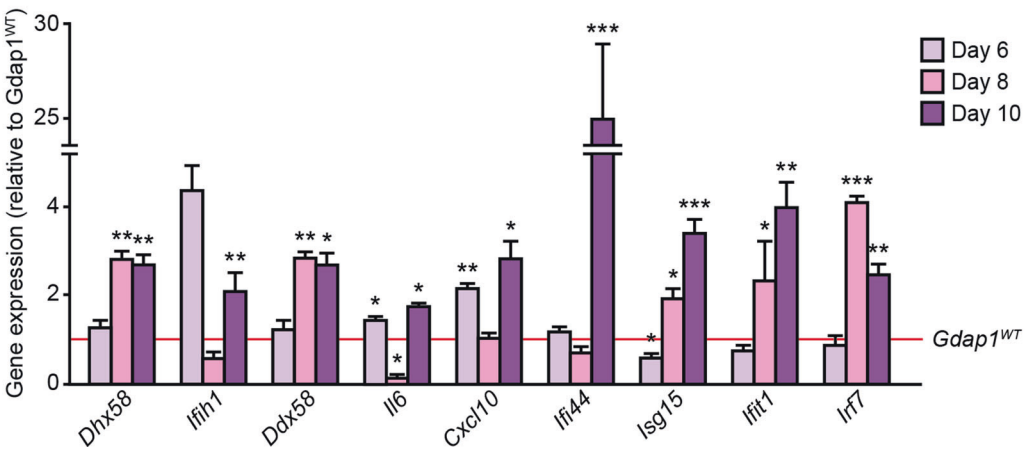

Fig. 6 Innate immune response activation in *Gdap1*$^{-/-}$ iPSCs differentiated into MNs. A Gene ontology analysis (GO) comparing *Gdap1*^{WT} and *Gdap1*$^{-/-}$ MEFs gene expression profiles. Activated (top, log positive ratio) or inactivated (bottom, log negative ratio) pathways are shown. **B** iPSCs were set up to differentiate into MNs and relative gene expression was evaluated at the indicated times: d6 (EBs), d8 (1 day after plating), d10 (3 days after plating). Data are represented as the mean ± SEM from at least three independent experiments. The one-tailed Student's t-test was used to assess statistical significance between genotypes (*$P < 0.05$; **$P < 0.01$; ***$P < 0.001$).

possibly due to ATP5B protein downregulation. This altered metabolic profile of *Gdap1*$^{-/-}$ cells correlates with a dysfunctional mitochondrial state that is likely a key factor in GDAP1 deficiency-associated cellular defects in CMT disease.

Oxidative stress has been proposed as a crucial element in various neurological disorders [52]. GDAP1 contains characteristic GST domains and, in agreement with our data, overexpression of GDAP1 stabilized glutathione concentration, reduced superoxide anion production and provided resistance to cell death induced by oxidative stress in HT22 cells [17]. Furthermore, another study demonstrated that the absence of *Gdap1* increased oxidative stress in mice [23]. In this regard, dominant mutations in *GDAP1* (associated with CMT2K) usually fall on the GST domains of the protein [53] and it has been suggested that these mutations are responsible for ROS overproduction [18].

Neuronal cell death is a hallmark of neurodegenerative diseases [54]. Here we show that *Gdap1*$^{-/-}$ MNs have a fragile phenotype prone to degeneration associated with activation of the p38α MAPK, a key player in apoptotic cell death [55]. In fact, it has been suggested that persistent activation of p38 and JNK MAPKs may participate in neuronal apoptosis in neurodegenerative pathologies [56–58], including CMT2B [59].

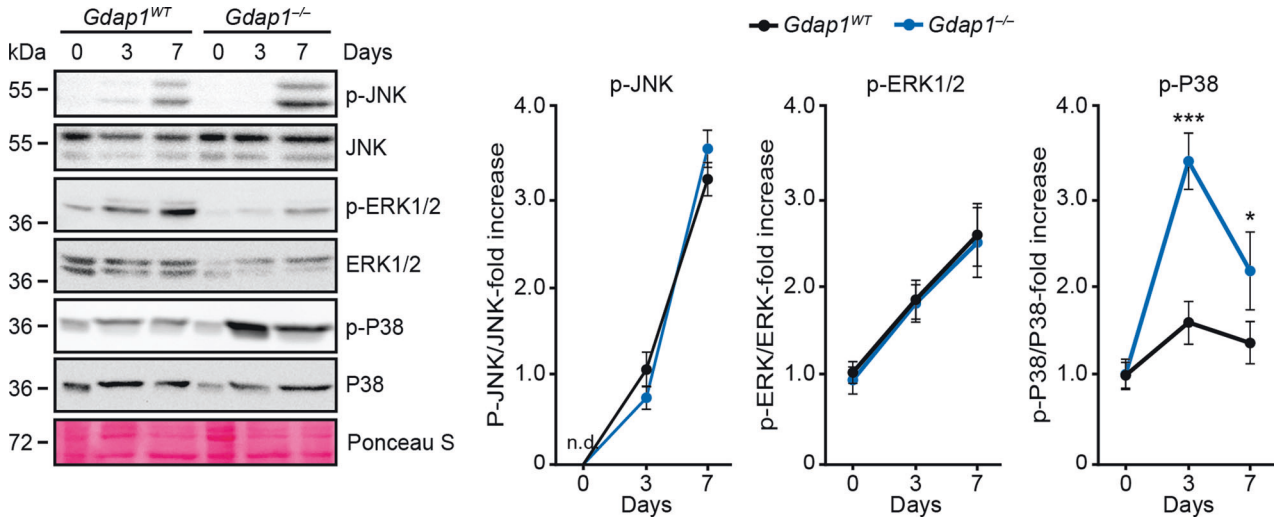

Fig. 7 MAPK activation profile during WT and *Gdap1*$^{-/-}$ MN differentiation. Left: cell lysates from undifferentiated or MN-differentiated iPSCs were analyzed by immunoblotting at the indicated timepoints. Loading control: Ponceau-S staining. Right: graphs showing quantification of MAPK phosphorylation ($n = 3$). Data are represented as the mean ± SEM from at least three independent experiments. The one-tailed Student's t-test was used to assess statistical significance between genotypes (*$P < 0.05$; ***$P < 0.001$).

Also, it has been observed that chronic neuroinflammation is present in several neurodegenerative diseases [60–63]. Interestingly, our results show that Gdap1-null MNs exhibit activation of the innate immune response. In agreement, *Gdap1*$^{-/-}$ mice presented chronic neuroinflammation in the spinal cord and sciatic nerve [64]. The chronic inflammation observed was suggested to be part of the pathophysiology of the axonal form of *GDAP1*-linked CMT variants.

HK1 and HK2 proteins localize to the mitochondrial surface by direct interaction with the voltage-dependent anion channel (VDAC). It is known that the interaction of VDAC with these hexokinases protects cells from mitochondrial ROS production [65] and suppresses the pro-apoptotic interactions between VDAC and members of the BCL family, which lead to the opening of the mitochondrial permeability transition pore and the release of mitochondrial contents to cytosol [66–69]. Indeed, each of these processes have been previously implicated in inflammasome activation to mount an innate immune response [70]. As lack of *Gdap1* leads to downregulation of *Hk2* in MNs, the possibility that GDAP1 deficiency could lead to the opening of the mitochondrial permeability transition pore thus mounting the innate immune response is a possibility that deserves further investigation, as it may provide the molecular link to MN degeneration in CMT2, opening therefore new avenues for its therapeutical intervention.

MATERIALS AND METHODS

Cell culture, differentiation assays, reagents, and plasmids

iPSC lines were cultured in the presence of hLIF as previously described [33]. Motor neuron iPSC reporters were generated by electroporation of the *pMnx1*-EFGP reporter [29]. Differentiation of iPSC lines into MNs was carried out as described [29, 31]. Different iPS cell clones of both genotypes were included in all the experiments shown in this manuscript. All iPS cell clones used in this manuscript did not show any appreciable bias in neither their growth or differentiation properties [30]. Further details are provided in supplementary information.

Immunofluorescence and flow cytometry

Cells were fixed in 4% PFA (in PBS), permeabilized with 0.5% Triton X-100 in PBS, blocked with 3% BSA in PBS, and incubated overnight at 4 °C with indicated primary antibodies. Next day, samples were washed with PBS and incubated with secondary antibodies in the dark. After washing with PBS, cells were incubated with Hoechst 33342 (Molecular Probes, H3570) as nuclear counterstaining, washed with PBS, rinsed with water, and mounted. For analysis of mitochondrial membrane potential, cells were incubated with 10 nm TMRM (Life Technologies, T668) for 20 min at 37 °C in the dark. For the analysis of mitochondrial superoxide, cells were incubated with 5 µM MitoSOX (Thermo Fisher Scientific, M36008) for 10 min at 37 °C in the dark. Colocalization of Tom20 and Lc3b staining was evaluated by calculating the Pearson Correlation Coefficient (PCC) using the freely available JACoP plug-in (http://rsb.info.nih.gov/ij/plugins/track/jacop.html) for ImageJ analysis software, as previously described [71]. Antibodies are listed in supplementary information.

For assessing mitochondrial membrane potential and ROS levels by flow cytometry, EBs were trypsinised and resuspended in 2% FBS-PBS solution, and incubated with TMRM 10 nm (Life Technologies, T668) or 5 µM MitoSOX (Thermo Fisher Scientific, M36008) for 5 min at 37 °C in the dark. Measurements were taken with the BD FACSCanto II cytometer (BD Biosciencies) and results analyzed with FlowJo (Tree Star, Inc.). Data from at least 10,000 cell events per sample were acquired.

Live-cell imaging

Images of MNs in culture were captured using an IN-Cell Analyzer 2000 microscope (GE Healthcare, Inc.) with a 40X objective under controlled atmosphere conditions (5% CO_2, 37 °C). Cells were imaged every hour (24 h total). Images were analyzed using ImageJ software (National Institutes of Health) and the number of neurites per soma was quantified by direct observation of the images.

Western blot

Cells from EBs were lysed on ice in RIPA buffer (50 mM Tris pH 7.5, 150 mM NaCl, 0.1% SDS, 1% Triton X-100, 0.5% sodium deoxycholate) supplemented with phosphatase and protease inhibitors. Cellular lysates were used for immunoblotting with indicated antibodies. Signals in membranes were detected using ECL prime (Amersham) and images automatically captured in an Alliance Mini HD9 (UVITEC, UK) system. Acquired images were analyzed with ImageJ. Antibodies used are listed in supplementary information. For LC3B immunoblots, cells were incubated with 50 µM Chloroquine (Sigma-Aldrich, C6628) for 4 h prior lysis with ice-cold RIPA buffer. Uncropped blots can be found in Supplementary materials.

RNA isolation and RT-qPCR analysis

Total RNA was extracted using TRI reagent (Sigma-Aldrich, T9424) and cDNA synthesized using SuperScript III reverse transcriptase (ThermoFisher Scientific, 10432122). 2–3 µl of cDNA were amplified in the StepOnePlus Real-Time PCR system (Applied Biosystems) using SYBR Premix ExTaq (Takara, RR420A). Each RT-qPCR assay was performed in duplicate and repeated at least 3 times. Primers used are listed in supplementary information.

Microarray data analysis

Microarray data has been described [30]. In-silico analysis was carried out for the Gene Ontology (GO) terms and for the Kyoto Encyclopedia of Genes and Genomes (KEGG) Pathways using a logistic regression.

Extracellular metabolic flux analysis

Basal and uncoupled oxygen consumption rates (OCR), or extracellular acidification rates (ECAR), were measured using a Seahorse bioanalyzer (XF96) and the Mito or Glycolysis stress test kits (both from Seahorse Bioscience, Millipore), respectively, following the manufacturer recommendations. Measurements were normalized to total number of cells per well by fluorescence microscopy on a replica-seeded plate stained with Hoechst 33342. Each experiment was conducted in quadruplicate and repeated at least 3 times. Further details can be found in supplementary information.

Statistics

Where indicated, Student's *t*-test was used to estimate statistical significance between two categories. Relative values (percentages) were normalized using arcsine transformation before carrying out their statistical comparison. In all assays at least 3 different iPS cell clones ($n \geq 3$) per genotype were tested. Each data point was independently repeated at least three times. These independently repeated experiments were considered as replicates for statistical analysis. In all figures, panels display representative images from 1–2 different iPS cell clones. Bar diagrams displaying numerical results were obtained from at least 3 independent iPS cell clones (*n*) from each genotype.

DATA AVAILABILITY

Data supporting the present study are available from the correspondence author upon reasonable request.

REFERENCES

1. Gutmann L, Shy M. Update on Charcot-Marie-Tooth disease. Curr Opin Neurol. 2015;28:462–7. https://pubmed.ncbi.nlm.nih.gov/26263471/.
2. Mathis S, Goizet C, Tazir M, Magdelaine C, Lia AS, Magy L, et al. Charcot-Marie-Tooth diseases: an update and some new proposals for the classification. J Med Genet. 2015;52:681–90. https://pubmed.ncbi.nlm.nih.gov/26246519/.
3. McGrath MC. Charcot-Marie-Tooth 1A: A narrative review with clinical and anatomical perspectives. Clin Anat. 2016;29:547–54. https://pubmed.ncbi.nlm.nih.gov/26457477/.
4. Pareyson D, Saveri P, Pisciotta C. New developments in Charcot-Marie-Tooth neuropathy and related diseases. Curr Opin Neurol. 2017;30:471–80. https://pubmed.ncbi.nlm.nih.gov/28678038/.
5. Laurá M, Pipis M, Rossor AM, Reilly MM. Charcot-Marie-Tooth disease and related disorders: an evolving landscape. Curr Opin Neurol. 2019;32:641–50. https://pubmed.ncbi.nlm.nih.gov/31343428/.
6. McCray BA, Scherer SS. Axonal Charcot-Marie-Tooth disease: from common pathogenic mechanisms to emerging treatment opportunities. Neurotherapeutics. 2021;18:2269–85. https://pubmed.ncbi.nlm.nih.gov/34606075/.
7. Pedrola L, Espert A, Valdés-Sánchez T, Sánchez-Piris M, Sirkowski EE, Scherer SS, et al. Cell expression of GDAP1 in the nervous system and pathogenesis of Charcot-Marie-Tooth type 4A disease. J Cell Mol Med. 2008;12:679–89. https://pubmed.ncbi.nlm.nih.gov/18021315/.
8. Niemann A, Ruegg M, la Padula V, Schenone A, Suter U. Ganglioside-induced differentiation associated protein 1 is a regulator of the mitochondrial network: new implications for Charcot-Marie-Tooth disease. J Cell Biol. 2005;170:1067–78. https://pubmed.ncbi.nlm.nih.gov/16172208/.
9. Azzedine H, Ruberg M, Ente D, Gilardeau C, Périé S, Wechsler B, et al. Variability of disease progression in a family with autosomal recessive CMT associated with a S194X and new R310Q mutation in the GDAP1 gene. Neuromuscul Disord Elsevier Ltd. 2003;13:341–6.
10. Cassereau J, Chevrollier A, Gueguen N, Desquiret V, Verny C, Nicolas G, et al. Mitochondrial dysfunction and pathophysiology of Charcot-Marie-Tooth disease involving GDAP1 mutations. Exp Neurol. 2011;227:31–41. https://pubmed.ncbi.nlm.nih.gov/20849849/.
11. Auranen M, Ylikallio E, Toppila J, Somer M, Kiuru-Enari S, Tyynismaa H. Dominant GDAP1 founder mutation is a common cause of axonal Charcot-Marie-Tooth disease in Finland. Neurogenet. 2013;14:123–32. https://pubmed.ncbi.nlm.nih.gov/23456260/.
12. Baxter RV, Othmane K, ben, Rochelle JM, Stajich JE, Hulette C, Dew-Knight S, et al. Ganglioside-induced differentiation-associated protein-1 is mutant in Charcot-Marie-Tooth disease type 4A/8q21. Nat Genet. 2002;30:21–2. https://pubmed.ncbi.nlm.nih.gov/11743579/.
13. Cuesta A, Pedrola L, Sevilla T, García-Planells J, Chumillas MJ, Mayordomo F, et al. The gene encoding ganglioside-induced differentiation-associated protein 1 is mutated in axonal Charcot-Marie-Tooth type 4A disease.Nat Genet. 2002;30:22–5. https://pubmed.ncbi.nlm.nih.gov/11743580/.
14. Nelis E, Erdem S, van den Bergh PYK, Belpaire-Dethiou MC, Ceuterick C, van Gerwen V, et al. Mutations in GDAP1: autosomal recessive CMT with demyelination and axonopathy. Neurol. 2002;59:1865–72. https://pubmed.ncbi.nlm.nih.gov/12499475/.
15. Fabrizi GM, Cavallaro T, Angiari C, Cabrini I, Taioli F, Malerba G, et al. Charcot-Marie-Tooth disease type 2E, a disorder of the cytoskeleton. Brain. 2007;130:394–403. https://pubmed.ncbi.nlm.nih.gov/17052987/.
16. Marco A, Cuesta A, Pedrola L, Palau F, Marín I. Evolutionary and structural analyses of GDAP1, involved in Charcot-Marie-Tooth disease, characterize a novel class of glutathione transferase-related genes. Mol Biol Evol. 2004;21:176–87. https://pubmed.ncbi.nlm.nih.gov/14595091/.
17. Noack R, Frede S, Albrecht P, Henke N, Pfeiffer A, Knoll K, et al. Charcot-Marie-Tooth disease CMT4A: GDAP1 increases cellular glutathione and the mitochondrial membrane potential. Hum Mol Genet. 2012;21:150–62. https://pubmed.ncbi.nlm.nih.gov/21965300/.
18. Cassereau J, Chevrollier A, Codron P, Goizet C, Gueguen N, Verny C, et al. Oxidative stress contributes differentially to the pathophysiology of Charcot-Marie-Tooth disease type 2K. Exp Neurol; 2020 [cited 2022 Sep 4];323. Available from: https://pubmed.ncbi.nlm.nih.gov/31655048/.
19. Pla-Martín D, Rueda CB, Estela A, Sánchez-Piris M, González-Sánchez P, Traba J, et al. Silencing of the Charcot-Marie-Tooth disease-associated gene GDAP1 induces abnormal mitochondrial distribution and affects Ca2+ homeostasis by reducing store-operated Ca2+ entry. Neurobiol Dis. 2013;55:140–51. https://pubmed.ncbi.nlm.nih.gov/23542510/.
20. González-Sánchez P, Satrústegui J, Palau F, del Arco A Calcium Deregulation and Mitochondrial Bioenergetics in GDAP1-Related CMT Disease. Int J Mol Sci. 2019 [cited 2022 Sep 3];20. Available from: https://pubmed.ncbi.nlm.nih.gov/30669311/.
21. Civera-Tregón A, Domínguez L, Martínez-Valero P, Serrano C, Vallmitjana A, Benítez R, et al. Mitochondria and calcium defects correlate with axonal dysfunction in GDAP1-related Charcot-Marie-Tooth mouse model. Neurobiol Dis. 2021 [cited 2022 Sep 3];152. Available from: https://pubmed.ncbi.nlm.nih.gov/33582224/.
22. Barneo-Muñoz M, Juárez P, Civera-Tregón A, Yndriago L, Pla-Martin D, Zenker J, et al. Lack of GDAP1 induces neuronal calcium and mitochondrial defects in a knockout mouse model of charcot-marie-tooth neuropathy. PLoS Genet. 2015 [cited 2022 Sep 4];11. Available from: https://pubmed.ncbi.nlm.nih.gov/25860513/.
23. Niemann A, Huber N, Wagner KM, Somandin C, Horn M, Lebrun-Julien F, et al. The Gdap1 knockout mouse mechanistically links redox control to Charcot-Marie-Tooth disease. Brain. 2014;137:668–82. https://pubmed.ncbi.nlm.nih.gov/24480485/.
24. del Amo VL, Seco-Cervera M, García-Giménez JL, Whitworth AJ, Pallardó FV, Galindo MI. Mitochondrial defects and neuromuscular degeneration caused by altered expression of Drosophila Gdap1: implications for the Charcot-Marie-Tooth neuropathy. Hum Mol Genet. 2015;24:21–36. https://pubmed.ncbi.nlm.nih.gov/25122658/.
25. Faye PA, Vedrenne N, Miressi F, Rassat M, Romanenko S, Richard L, et al. Optimized protocol to generate spinal motor neuron cells from induced pluripotent stem cells from Charcot Marie Tooth patients. Brain Sci. 2020;10:1–14. https://pubmed.ncbi.nlm.nih.gov/32605002/.
26. Miressi F, Benslimane N, Favreau F, Rassat M, Richard L, Bourthoumieu S, et al. GDAP1 involvement in mitochondrial function and oxidative stress, investigated in a Charcot-Marie-Tooth model of hiPSCs-derived motor neurons. Biomedicines. 2021 [cited 2022 Sep 3];9. Available from: https://pubmed.ncbi.nlm.nih.gov/34440148/.
27. Wolf C, Pouya A, Bitar S, Pfeiffer A, Bueno D, Rojas-Charry L, et al. GDAP1 loss of function inhibits the mitochondrial pyruvate dehydrogenase complex by altering the actin cytoskeleton. Commun Biol. 2022 [cited 2022 Sep 3];5. Available from: https://pubmed.ncbi.nlm.nih.gov/35662277/.
28. Rzepnikowska W, Kochański A. A role for the GDAP1 gene in the molecular pathogenesis of Charcot-Marie-Tooth disease. Acta Neurobiol Exp (Wars). 2018;78:1–13. https://pubmed.ncbi.nlm.nih.gov/29694336/.
29. Wichterle H, Lieberam I, Porter JA, Jessell TM. Directed differentiation of embryonic stem cells into motor neurons. Cell [Internet] Cell. 2002;110:385–97. https://pubmed.ncbi.nlm.nih.gov/12176325/.

30. Prieto J, León M, Ponsoda X, García-García F, Bort R, Serna E, et al. Dysfunctional mitochondrial fission impairs cell reprogramming. Cell Cycle. 2016;15:3240–50. https://pubmed.ncbi.nlm.nih.gov/27755531/.
31. Peljto M, Dasen JS, Mazzoni EO, Jessell TM, Wichterle H. Functional diversity of ESC-derived motor neuron subtypes revealed through intraspinal transplantation. Cell Stem Cell. 2010;7:355–66. https://pubmed.ncbi.nlm.nih.gov/20804971/.
32. Niemann A, Wagner KM, Ruegg M, Suter U. GDAP1 mutations differ in their effects on mitochondrial dynamics and apoptosis depending on the mode of inheritance. Neurobiol Dis. 2009;36:509–20. https://pubmed.ncbi.nlm.nih.gov/19782751/.
33. Prieto J, León M, Ponsoda X, Sendra R, Bort R, Ferrer-Lorente R, et al. Early ERK1/2 activation promotes DRP1-dependent mitochondrial fission necessary for cell reprogramming. Nat Commun. 2016;7:11124 https://pubmed.ncbi.nlm.nih.gov/27030341/.
34. Hantke J, Chandler D, King R, Wanders RJA, Angelicheva D, Tournev I, et al. A mutation in an alternative untranslated exon of hexokinase 1 associated with hereditary motor and sensory neuropathy - Russe (HMSNR). Eur J Hum Genet. 2009;17:1606–14. https://pubmed.ncbi.nlm.nih.gov/19536174/.
35. Gabrikova D, Mistrik M, Bernasovska J, Bozikova A, Behulova R, Tothova I, et al. Founder mutations in NDRG1 and HK1 genes are common causes of inherited neuropathies among Roma/Gypsies in Slovakia. J Appl Genet. 2013;54:455–60. https://pubmed.ncbi.nlm.nih.gov/23996628/.
36. Sevilla T, Martínez-Rubio D, Márquez C, Paradas C, Colomer J, Jaijo T, et al. Genetics of the Charcot-Marie-Tooth disease in the Spanish Gypsy population: the hereditary motor and sensory neuropathy-Russe in depth. Clin Genet. 2013;83:565–70. https://pubmed.ncbi.nlm.nih.gov/22978647/.
37. Dong C, Davis RJ, Flavell RA. MAP kinases in the immune response. Annu Rev Immunol. 2002;20:55–72. https://pubmed.ncbi.nlm.nih.gov/11861597/.
38. Son Y, Cheong Y-K, Kim N-H, Chung H-T, Kang DG, Pae H-O. Mitogen-activated protein kinases and reactive oxygen species: how can ROS activate MAPK pathways? J Signal Transduct. 2011;2011:1–6. https://pubmed.ncbi.nlm.nih.gov/21637379/.
39. Son Y, Kim S, Chung HT, Pae HO. Reactive oxygen species in the activation of MAP kinases. Methods Enzymol. 2013;528:27–48. https://pubmed.ncbi.nlm.nih.gov/23849857/.
40. Pedrola L, Espert A, Wu X, Claramunt R, Shy ME, Palau F. GDAP1, the protein causing Charcot-Marie-Tooth disease type 4A, is expressed in neurons and is associated with mitochondria. Hum Mol Genet. 2005;14:1087–94. https://pubmed.ncbi.nlm.nih.gov/15772096/.
41. Huber N, Guimaraes S, Schrader M, Suter U, Niemann A. Charcot-Marie-Tooth disease-associated mutants of GDAP1 dissociate its roles in peroxisomal and mitochondrial fission. EMBO Rep. 2013;14:545–52. https://pubmed.ncbi.nlm.nih.gov/23628762/.
42. Park J, Lee J, Choi C Mitochondrial network determines intracellular ROS dynamics and sensitivity to oxidative stress through switching inter-mitochondrial messengers. PLoS ONE. 2011 [cited 2022 Sep 3];6. Available from: https://pubmed.ncbi.nlm.nih.gov/21829717/.
43. Dan Dunn J, Alvarez LAJ, Zhang X, Soldati T. Reactive oxygen species and mitochondria: a nexus of cellular homeostasis. Redox Biol. 2015;6:472–85. https://pubmed.ncbi.nlm.nih.gov/26432659/.
44. Twig G, Elorza A, Molina AJA, Mohamed H, Wikstrom JD, Walzer G, et al. Fission and selective fusion govern mitochondrial segregation and elimination by autophagy. EMBO J. 2008;27:433–46. https://pubmed.ncbi.nlm.nih.gov/18200046/.
45. Rodriguez-Enriquez S, He L, Lemasters JJ. Role of mitochondrial permeability transition pores in mitochondrial autophagy. Int J Biochem Cell Biol. 2004;36:2463–72. https://pubmed.ncbi.nlm.nih.gov/15325585/.
46. Kim I, Rodriguez-Enriquez S, Lemasters JJ. Selective degradation of mitochondria by mitophagy. Arch Biochem Biophys. 2007;462:245–53. https://pubmed.ncbi.nlm.nih.gov/17475204/.
47. Kanki T, Wang K, Klionsky DJ. A genomic screen for yeast mutants defective in mitophagy. Autophagy. 2010;6:278–80. https://pubmed.ncbi.nlm.nih.gov/20364111/.
48. Poole AC, Thomas RE, Yu S, Vincow ES, Pallanck L The mitochondrial fusion-promoting factor mitofusin is a substrate of the PINK1/parkin pathway. PLoS ONE. 2010 [cited 2022 Sep 3];5. Available from: https://pubmed.ncbi.nlm.nih.gov/20383334/.
49. Ziviani E, Tao RN, Whitworth AJ. Drosophila parkin requires PINK1 for mitochondrial translocation and ubiquitinates mitofusin. Proc Natl Acad Sci USA. 2010;107:5018–23. https://pubmed.ncbi.nlm.nih.gov/20194754/.
50. Federico A, Cardaioli E, da Pozzo P, Formichi P, Gallus GN, Radi E. Mitochondria, oxidative stress and neurodegeneration. J Neurol Sci. 2012;322:254–62. https://pubmed.ncbi.nlm.nih.gov/22669122/.
51. Fantin VR, St-Pierre J, Leder P. Attenuation of LDH-A expression uncovers a link between glycolysis, mitochondrial physiology, and tumor maintenance. Cancer Cell. 2006;9:425–34. https://pubmed.ncbi.nlm.nih.gov/16766262/.
52. Singh A, Kukreti R, Saso L, Kukreti S. Oxidative stress: a key modulator in neurodegenerative diseases. Molecules. 2019 [cited 2022 Sep 3];24. Available from: https://pubmed.ncbi.nlm.nih.gov/31013638/.
53. Crimella C, Tonelli A, Airoldi G, Baschirotto C, D'Angelo MG, Bonato S, et al. The GST domain of GDAP1 is a frequent target of mutations in the dominant form of axonal Charcot Marie Tooth type 2K. J Med Genet. 2010;47:712–6. https://pubmed.ncbi.nlm.nih.gov/20685671/.
54. Seifert G, Schilling K, Steinhäuser C. Astrocyte dysfunction in neurological disorders: a molecular perspective. Nat Rev Neurosci. 2006;7:194–206. https://pubmed.ncbi.nlm.nih.gov/16495941/.
55. Miller AL, Webb MS, Copik AJ, Wang Y, Johnson BH, Kumar R, et al. p38 Mitogen-activated protein kinase (MAPK) is a key mediator in glucocorticoid-induced apoptosis of lymphoid cells: correlation between p38 MAPK activation and site-specific phosphorylation of the human glucocorticoid receptor at serine 211. Mol Endocrinol. 2005;19:1569–83. https://pubmed.ncbi.nlm.nih.gov/15817653/.
56. Hensley K, Floyd RA, Zheng NY, Nael R, Robinson KA, Nguyen X, et al. p38 kinase is activated in the Alzheimer's disease brain. J Neurochem. 1999;72:2053–8. [cited 2022 Sep 3]Available from https://pubmed.ncbi.nlm.nih.gov/10217284/.
57. Tortarolo M, Veglianese P, Calvaresi N, Botturi A, Rossi C, Giorgini A, et al. Persistent activation of p38 mitogen-activated protein kinase in a mouse model of familial amyotrophic lateral sclerosis correlates with disease progression. Mol Cell Neurosci. 2003;23:180–92. https://pubmed.ncbi.nlm.nih.gov/12812752/.
58. Gui C, Ren Y, Chen J, Wu X, Mao K, Li H, et al. p38 MAPK-DRP1 signaling is involved in mitochondrial dysfunction and cell death in mutant A53T α-synuclein model of Parkinson's disease. Toxicol Appl Pharmacol [Internet]. Toxicol Appl Pharmacol. 2020 [cited 2022 Sep 3];388. Available from: https://pubmed.ncbi.nlm.nih.gov/31881179/.
59. BasuRay S, Mukherjee S, Romero EG, Seaman MNJ, Wandinger-Ness A. Rab7 mutants associated with Charcot-Marie-Tooth disease cause delayed growth factor receptor transport and altered endosomal and nuclear signaling. J Biol Chem [Internet] J Biol Chem. 2013;288:1135–49. https://pubmed.ncbi.nlm.nih.gov/23188822/.
60. Orr CF, Rowe DB, Halliday GM. An inflammatory review of Parkinson's disease. Prog Neurobiol [Internet] Prog Neurobiol. 2002;68:325–40. https://pubmed.ncbi.nlm.nih.gov/12531233/.
61. Weydt P, Möller T. Neuroinflammation in the pathogenesis of amyotrophic lateral sclerosis. Neuroreport. 2005;16:527–31. https://pubmed.ncbi.nlm.nih.gov/15812300/.
62. Möller T. Neuroinflammation in Huntington's disease. J Neural Transm (Vienna). 2010;117:1001–8. https://pubmed.ncbi.nlm.nih.gov/20535620/.
63. Heppner FL, Ransohoff RM, Becher B. Immune attack: the role of inflammation in Alzheimer disease. Nat Rev Neurosci. 2015;16:358–72. https://pubmed.ncbi.nlm.nih.gov/25991443.
64. Fernandez-Lizarbe S, Civera-Tregón A, Cantarero L, Herrer I, Juarez P, Hoenicka J, et al. Neuroinflammation in the pathogenesis of axonal Charcot-Marie-Tooth disease caused by lack of GDAP1. Exp Neurol. 2019 [cited 2022 Sep 3];320. Available from: https://pubmed.ncbi.nlm.nih.gov/31271761/.
65. Da-Silva WS, Gómez-Puyou A, de Gómez-Puyou MT, Moreno-Sanchez R, de Felice FG, de Meis L, et al. Mitochondrial bound hexokinase activity as a preventive antioxidant defense: steady-state ADP formation as a regulatory mechanism of membrane potential and reactive oxygen species generation in mitochondria. J Biol Chem. 2004;279:39846–55. https://pubmed.ncbi.nlm.nih.gov/15247300/.
66. Pastorino JG, Hoek JB. Regulation of hexokinase binding to VDAC. J Bioenerg Biomembr. 2008;40:171–82. https://pubmed.ncbi.nlm.nih.gov/18683036/.
67. Majewski N, Nogueira V, Bhaskar P, Coy PE, Skeen JE, Gottlob K, et al. Hexokinase-mitochondria interaction mediated by Akt is required to inhibit apoptosis in the presence or absence of Bax and Bak. Mol Cell. 2004;16:819–30. https://pubmed.ncbi.nlm.nih.gov/15574336/.
68. Chiara F, Castellaro D, Marin O, Petronilli V, Brusilow WS, Juhaszova M, et al. Hexokinase II detachment from mitochondria triggers apoptosis through the permeability transition pore independent of voltage-dependent anion channels. PLoS ONE. 2008 [cited 2022 Sep 3];3. Available from: https://pubmed.ncbi.nlm.nih.gov/18350175/.
69. Rasola A, Sciacovelli M, Pantic B, Bernardi P. Signal transduction to the permeability transition pore. FEBS Lett. 2010;584:1989–96. https://pubmed.ncbi.nlm.nih.gov/20153328/.
70. Wolf AJ, Reyes CN, Liang W, Becker C, Shimada K, Wheeler ML, et al. Hexokinase Is an innate immune receptor for the detection of bacterial peptidoglycan. Cell [Internet]. 2016;166:624.
71. Bolte S, Cordelières FP. A guided tour into subcellular colocalization analysis in light microscopy. J Microsc. 2006;224:213–32. https://pubmed.ncbi.nlm.nih.gov/17210054/.

ACKNOWLEDGEMENTS

We thank Austin Smith and Thomas Jessell for the pPYCAG-IP and pHb9-EGFP vectors, respectively. We thank Dr. Lisa Sevilla for critically reading the manuscript. We are indebted to Prof. Erwin Knecht, Prof. Pascual Sanz and Prof. Ramón Sendra for their help with LC3B immunoblotting.

AUTHOR CONTRIBUTIONS

ML carried out most of the experimental work. MM and RS helped with immunoblotting design. XP assisted in microscopy experiments. MB-M and FP generated and carried out the phenotype analysis of the *Gdap1* knockout mice. FG-G and JD carried out the in-silico transcriptome analysis. JP collaborated in the experimental work and provided with a draft of the manuscript. JCIB and JT designed the experiments, supervised the work, and prepared the final version of the manuscript. All authors participated in the discussion of the results.

FUNDING

This work was funded by a collaborative joint project awarded by IRDiRC and funded by ISCIII grant IR11/TREAT-CMT, Instituto de Salud Carlos III (to JT and FP). JP was supported by postdoctoral fellowships from Fundación Alfonso Martín Escudero and Generalitat Valenciana (VALi+d 2019 program).

COMPETING INTERESTS

The authors declare no competing interests.

ADDITIONAL INFORMATION

Supplementary information The online version contains supplementary material available at https://doi.org/10.1038/s41420-023-01531-w.

Correspondence and requests for materials should be addressed to Josema Torres.

Reprints and permission information is available at http://www.nature.com/reprints

Publisher's note Springer Nature remains neutral with regard to jurisdictional claims in published maps and institutional affiliations.